THE JOURNAL OF BIOLOGICAL CHEMISTRY VOL. 283, NO. 31, pp. 21550–21558, August 1, 2008

Structural Determinants Underlying the Temperature-sensitive Nature of a Gα Mutant in Asymmetric Cell Division of *Caenorhabditis elegans*[*] [S]

Received for publication, April 21, 2008, and in revised form, June 2, 2008 Published, JBC Papers in Press, June 2, 2008, DOI 10.1074/jbc.M803023200

Christopher A. Johnston[‡1,2], Katayoun Afshar[§1], Jason T. Snyder[‡], Gregory G. Tall[¶3], Pierre Gönczy[§‖], David P. Siderovski[‡4], and Francis S. Willard[‡]**

*From the [‡]Department of Pharmacology and **Lineberger Comprehensive Cancer Center, University of North Carolina, Chapel Hill, North Carolina 27599, the [§]Swiss Institute for Experimental Cancer Research and [‖]School of Life Sciences, Swiss Federal Institute of Technology, 1066 Lausanne, Switzerland, and the [¶]Department of Pharmacology and Physiology, University of Rochester School of Medicine and Dentistry, Rochester, New York 14642*

Heterotrimeric G-proteins are integral to a conserved regulatory module that influences metazoan asymmetric cell division (ACD). In the *Caenorhabditis elegans* zygote, GOA-1 ($G\alpha_o$) and GPA-16 ($G\alpha_i$) are involved in generating forces that pull on astral microtubules and position the spindle asymmetrically. GPA-16 function has been analyzed *in vivo* owing notably to a temperature-sensitive allele *gpa-16*(*it143*), which, at the restrictive temperature, results in spindle orientation defects in early embryos. Here we identify the structural basis of *gpa-16*(*it143*), which encodes a point mutation (G202D) in the switch II region of GPA-16. Using $G\alpha_{i1}$(G202D) as a model in biochemical analyses, we demonstrate that high temperature induces instability of the mutant Gα. At the permissive temperature, the mutant Gα was stable upon GTP binding, but switch II rearrangement was compromised, as were activation state-selective interactions with regulators involved in ACD, including GoLoco motifs, RGS proteins, and RIC-8. We solved the crystal structure of the mutant Gα bound to GDP, which indicates a unique switch II conformation as well as steric constraints that suggest activated GPA-16(it143) is destabilized relative to wild type. Spindle severing in *gpa-16*(*it143*) embryos revealed that pulling forces are symmetric and markedly diminished at the restrictive temperature. Interestingly, pulling forces are asymmetric and generally similar in magnitude to wild type at the permissive temperature despite defects in the structure of GPA-16(it143). These normal pulling forces in *gpa-16*(*it143*) embryos at the permissive temperature were attributable to GOA-1 function, underscoring a complex interplay of Gα subunit function in ACD.

G-protein-coupled receptors (GPCRs)[5] mediate the actions of a variety of sensory and metabolic stimuli (1). Heterotrimeric G-proteins are molecular switches that transduce GPCR activation into intracellular changes and are composed of a Gα subunit and a Gβγ dimer (1, 2). GPCR-promoted activation of Gαβγ causes Gα to exchange GDP for GTP, which in turn causes Gα·GTP and Gβγ to dissociate. Gα·GTP and liberated Gβγ then regulate effector systems to alter cell physiology (1, 2). This canonical, GPCR-driven "G-protein cycle" is reset by the intrinsic GTP hydrolysis activity of Gα (1, 2).

A noncanonical, yet evolutionarily conserved, heterotrimeric G-protein regulatory module has been identified in *Caenorhabditis elegans*, *Drosophila*, and mammalian asymmetric cell division (ACD) that is important for generating diversity during development (1, 3–5). An initial step in ACD is generation of cell polarity. Cell fate determinants then segregate to different sides of the cell (3), and the mitotic spindle is positioned to permit proper distribution of determinants to daughter cells. Integral to accurate spindle positioning is a heterotrimeric G-protein module thought to be independent of GPCRs and involving GDP dissociation inhibitors (GoLoco motif proteins), guanine nucleotide exchange factors (*i.e.* RIC-8), and GTPase-accelerating proteins (RGS proteins) (1, 3, 4).

In the *Caenorhabditis elegans* zygote, G-protein involvement in ACD has been extensively studied using genetic and cell biological approaches (6). Two Gα subunits, GPA-16 and GOA-1, are important for generating pulling forces on astral microtubules critical for spindle positioning (7). These two Gα subunits are required for force generation in concert with the GoLoco motif proteins GPR-1/-2 and the coiled-coil protein LIN-5 (7). GPA-16 and GOA-1 exert partially redundant functions in ACD (8) but differ in some respects, *e.g.* RIC-8 is required for cortical localization of GPA-16 but not GOA-1 (9). The mechanisms by which GOA-1, GPA-16, and their binding partners mediate force generation during ACD are gradually being revealed (10–14) but remain incompletely understood.

Whereas the contribution of GOA-1 to ACD has been ana-

* This work was supported, in whole or in part, by National Institutes of Health Grant GM074268 (to D. P. S.). This work was also supported by Swiss National Science Foundation Grant 3100A0-102087 (to P. G.). The costs of publication of this article were defrayed in part by the payment of page charges. This article must therefore be hereby marked "*advertisement*" in accordance with 18 U.S.C. Section 1734 solely to indicate this fact.

The atomic coordinates and structure factors (code 2EBC) have been deposited in the Protein Data Bank, Research Collaboratory for Structural Bioinformatics, Rutgers University, New Brunswick, NJ (http://www.rcsb.org/).

[S] The on-line version of this article (available at http://www.jbc.org) contains supplemental Tables 1 and 2 and Movies S1–S6.

[1] Both authors contributed equally to this work.

[2] Supported by National Institutes of Health Fellowship GM076944.

[3] Supported by American Heart Association Grant 0325033Y.

[4] To whom correspondence should be addressed: 1106 M. E. Jones Bldg., CB 7365, Chapel Hill, NC 27599. Tel.: 919-843-9363; Fax: 919-966-5640; E-mail: dsiderov@med.unc.edu.

[5] The abbreviations used are: GPCR, G-protein coupled receptor; ACD, asymmetric cell division; GST, glutathione *S*-transferase; RU, resonance unit; GTPγS, guanosine 5′-3-*O*-(thio)triphosphate; RNAi, RNA interference; PDEγ, γ subunit of phosphodiesterase; cGMP, cyclic guanosine monophosphate.

lyzed solely using null alleles and RNAi-mediated inactivation, the role of GPA-16 in ACD was discovered using both RNAi and a unique temperature-sensitive allele *gpa-16*(*it143*). At 25 °C, 70% of *gpa-16*(*it143*) worms die during embryogenesis, with a significant proportion of adult escapers showing reversal of left-right body axis asymmetry (15). At 16 °C, only 2% of *gpa-16*(*it143*) worms die during embryogenesis (15), suggesting that GPA-16(it143) somehow supports function at the permissive temperature; however, an analysis of ACD in one-cell stage embryos at this particular temperature has not been conducted previously. The *gpa-16*(*it143*) allele encodes a point mutation causing a glycine 202 to aspartate (G202D) change in switch II of GPA-16 (15). We have used enzymology, crystallography, genetics, and cell biology to delineate the molecular mechanism underlying the critical contribution of this residue to GPA-16 function during ACD. Purifying GPA-16 from baculovirus-infected insect cells yields only micrograms of purified protein (9), preventing detailed biochemical and, especially, x-ray diffraction crystallographic structural studies. We have thus also examined the G202D mutation in the context of the most rigorously characterized and experimentally tractable Gα subunit that is most closely related to GPA-16, namely mammalian Gα_{i1} (9).

EXPERIMENTAL PROCEDURES

Materials—Unless otherwise specified, all reagents were of the highest purity obtainable from Sigma or Fisher (Pittsburgh, PA). Site-directed mutagenesis was conducted using the QuikChange mutagenesis kit (Stratagene, La Jolla, CA).

Protein Purification—Full-length His_6-tagged human Gα_{i1} (wild type and G202D) was purified as described (16, 17). Full-length His_6-tagged (wild type and G198D) chimeric Gα_t/Gα_{i1} subunits (18) were purified using standard chromatography methods (16, 19). Care was taken to keep all Gα subunits GDP-bound and at 4 °C throughout their respective purification processes. A GST fusion of rat Ric-8A was purified as described (20). Recombinant G$\beta_1\gamma_1$ dimer incorporating the biotinylation sequence was produced and purified as described (21), with DNA coding for the biotin ligase substrate motif (GLNDIFEAQKIEWHE) inserted upstream of the Gγ_1 coding sequence within the baculoviral shuttle vector pFASTBacHT (Invitrogen). Biotin protein ligase (BirA) was incubated with 50 μM G$\beta_1\gamma_1$ dimer for 24 h at 25 °C under the conditions described by the manufacturer (Avidity, Denver, CO). Resulting protein was buffer-exchanged into phosphate-buffered saline and stored at −80 °C. Full-length GST-tagged human PCP-2 was prepared as described (17). The RGS domain of rat RGS14 was prepared as a GST fusion protein as described (16). Wild type and scrambled RGS12 GoLoco motif synthetic peptides are described in Ref. 22. An N-terminal biotinylated peptide comprising amino acids 63–87 of bovine rod PDEγ is described in Ref. 23.

GTPγS Binding—[^{35}S]GTPγS (PerkinElmer Life Sciences) binding was measured using a filter binding assay as described previously (10). Rate constants were obtained by subtracting nonspecific binding (counts/min obtained in the presence of 100 μM unlabeled GTPγS) and fitting binding curves to a single exponential function in GraphPad Prism version 4.0 (San Diego, CA).

C. elegans Strains and RNAi Conditions—The N2 strain was used as wild type and maintained according to established procedures (24). The *gpa-16*(*it143*) strain (15) was maintained at 16 °C and shifted for 20–24 h to 25 °C before analysis at the restrictive temperature. For inactivation of *gpa-16* or *goa-1* by RNAi, bacterial feeding strains (10) were used to feed L3/L4 worms for 36 h at 25 °C or for 48 h at 16 °C.

Coimmunoprecipitation and Western Blot Analysis—Generation of worm embryonic extracts and coimmunoprecipitation experiments were performed as described (10) with the following modifications. For each experiment, ~1.5 mg of protein extract and 3 μg of GPA-16 antibodies (9) were utilized. As specified, GDP or GTPγS were included at final concentrations of 100 μM. For testing the interactions at 16 °C, lysates were incubated with antibodies and nucleotides at 16 °C for 40 min; 15 μl of protein G-Sepharose were added, and the incubation was continued at 4 °C overnight. Following immunoprecipitation, SDS-PAGE and Western blot analysis were performed according to standard procedures. RIC-8, GPR-1/2, and GPA-16 primary antibodies (9, 10) were diluted 1:1000 and horseradish peroxidase-conjugated goat anti-rabbit secondary antibodies (GE Healthcare) 1:2000; the signals were revealed by standard chemiluminescence (GE Healthcare).

Circular Dichroism—All CD experiments were performed in Buffer C (10 mM phosphate buffer (KH_2PO_4/K_2HPO_4), pH 7.5, 50 mM NaCl, 5 mM $MgCl_2$). For CD experiments, Gα subunits were purified as described (16, 19), but the final purification step was by Sephacryl S200 gel filtration (GE Healthcare) using Buffer C. For CD measurements, 50 μM of Gα subunits were loaded with 100 μM GDP or GTPγS at 15 °C for the times determined to give ≈100% binding, based on rate constants (see Fig. 1*B*). Proteins were then diluted to 4.4 μM in Buffer C and kept at 4 °C. CD was measured using a PiStar-180 spectrophotometer (Applied Photophysics, Surrey, UK). CD was measured at 208 nm (slits 4.0 nm) for 30 s at each temperature. The temperature ramp was conducted using 1 °C steps with a tolerance of ±0.2 °C. Apparent melting temperatures were calculated as the minima of first derivatives with respect to the reciprocal of temperature (25). First differential minima were calculated using Rt-Plot (version 2.7, Horst Reichert, Eppstein, Germany) using the Akima interpolation with a weighting of 1 (26).

Surface Plasmon Resonance—Surface plasmon resonance experiments with GST fusion proteins and biotinylated proteins were performed using a BIAcore 3000 (GE Healthcare) as described previously (19, 27). Sensor surfaces for all experiments were at 15 °C, and all proteins in the sample handler were kept at 4 °C. The eluent buffer was 10 mM HEPES, pH 7.4, 150 mM NaCl, 5 mM $MgCl_2$, and 0.005% (v/v) Nonidet P-40. Nucleotide-specific conformations of Gα were obtained by incubation with eluent buffer supplemented with 100 μM GDP (GDP) or 100 μM GTPγS (GTPγS) or 100 μM GDP, 20 mM NaF, and 30 μM $AlCl_3$ (GDP·AlF_4^-). GTPγS loading was conducted for 3 h at either 15 °C for Gα_{i1}(G202D) or 30 °C for Gα_{i1}(wild type). Loading levels for K_D determination experiments were as follows: biotin-G$\beta_1\gamma_1$ (1400 RU), GST-Ric-8A (300 RU), GST-PCP-2 (400 RU), GST-RGS14 (400 RU), and biotin-PDEγ (500

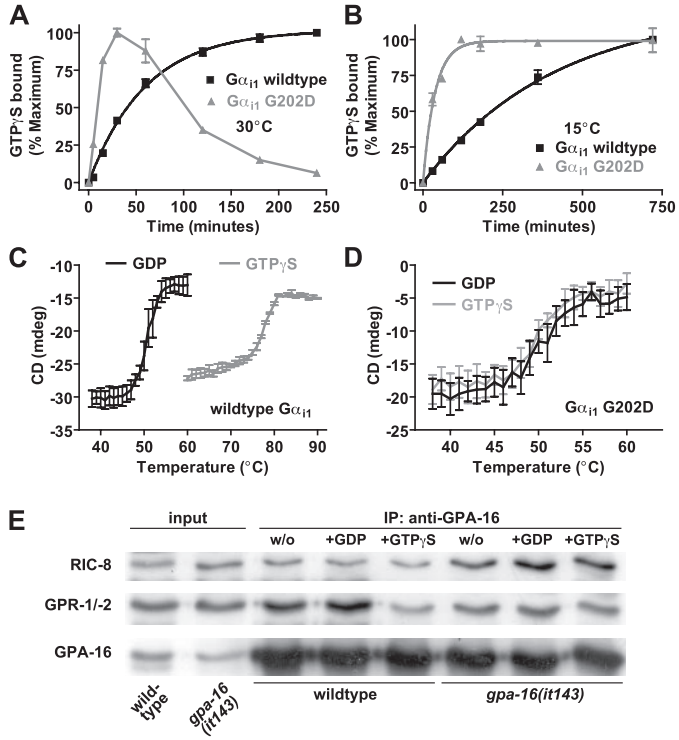

FIGURE 1. **Temperature-dependent nucleotide binding, protein stability, and protein interactions of wild type and G202D Gα subunits.** *A* and *B*, time course of GTPγS binding by wild type and G202D $G\alpha_{i1}$ measured at 30 °C (*A*) or 15 °C (*B*). 100 nM Gα was incubated with 1 μM [^{35}S]GTPγS, and bound nucleotide was measured at indicated times. Data were fit to single exponential association curves (95% confidence intervals in *brackets*) as follows: 30 °C wild type, 0.017 (0.015–0.019) min^{-1}; 30 °C G202D, data could not be fit; 15 °C wild type, 0.0025 (0.0021–0.0028) min^{-1}; 15 °C G202D, 0.027 (0.021–0.032) min^{-1}. *C* and *D*, CD in millidegrees (*mdeg*) of 4.4 μM wild type $G\alpha_{i1}$ (*C*) or G202D $G\alpha_{i1}$ (*D*) was measured at 208 nm in both GDP- and GTPγS-bound conformations. Thermal melting curves were generated by measuring CD values at 1 °C intervals. Data are graphed as mean ± S.E. The mean melting temperatures (S.E. in parenthesis; $n = 3$) for wild type $G\alpha_{i1}$ (*C*) were GDP 50.2 °C (0.4) and GTPγS 77.2 °C (0.4) and for G202D $G\alpha_{i1}$ (*D*) were GDP 49.5 °C (0.8) and GTPγS 50.1 °C (0.01). *E*, co-immunoprecipitation conducted at 16 °C using wild type or *gpa-16* (*it143*) embryonic extracts and GPA-16 antibody, either without (*w/o*) exogenous nucleotides or in the presence of 100 μM GDP or GTPγS. Immunoprecipitated material was analyzed by Western blot using antibodies against RIC-8, GPR-1/-2, or GPA-16. Input corresponds to 1/70 of starting material.

RU). Equilibrium binding K_D measurements were conducted at a flow rate of 20 μl/min using protocols described previously (28). Kinetic binding analyses were conducted as described previously (29). Nonspecific binding was determined using a biotinylated mNOTCH control peptide (27) and GST alone (19), respectively. Nonspecific binding was subtracted from experimental data to give binding curves using BIAevaluation software (version 3.0; Biacore).

Crystallization, Structure Determination, and Refinement—To aid crystallization of the labile G202D mutant of $G\alpha_{i1}$, we were careful to ensure strict temperature control throughout protein induction (14 °C), purification (4 °C), and crystallization (18 °C). Moreover, crystallization trials were conducted immediately following concentration of purified protein, as freeze-thawed protein was incapable of reproducing crystal growth. Crystals of $G\alpha_{i1}$(G202D) were obtained by vapor diffusion from hanging drops containing a 1:1 (v/v) ratio of protein solution (10–20 mg ml^{-1} in 50 mM HEPES buffer, pH 8.0, 1 mM

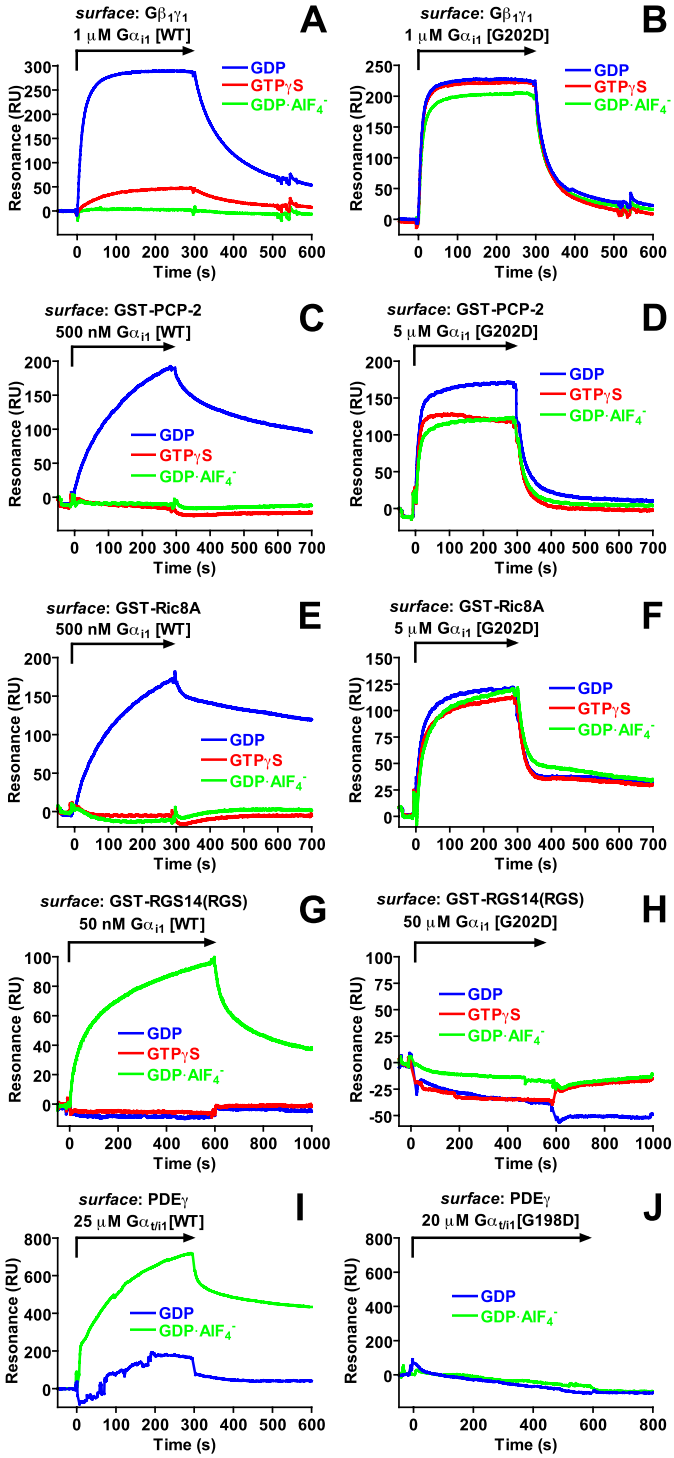

FIGURE 2. **Protein-protein interactions of wild type and Gly-to-Asp mutant Gα subunits.** Interactions between wild type (*WT*) or indicated Gly-to-Asp mutated Gα subunits and $G\beta_1\gamma_1$ (*A* and *B*), PCP-2 (*C* and *D*), Ric-8A (*E* and *F*), the RGS domain of RGS14 (*G* and *H*), and PDEγ(aa 63–87) (*I* and *J*) were measured using surface plasmon resonance. Proteins were immobilized using biotin-streptavidin coupling (*A, B, I,* and *J*) or anti-GST antibody capture (*C–H*). Indicated concentrations of Gα subunits in the GDP (*blue*), GTPγS (*red*), or GDP·AlF$_4^-$ (*green*) loaded forms were injected over biosensor surfaces at a flow rate of 20 μl/min as denoted by *arrows*. Binding curves were generated after subtracting nonspecific binding to mNOTCH peptide (*A, B, I,* and *J*) or GST (*C–H*) control surfaces.

EDTA, 100 μM GDP, and 5 mM dithiothreitol) to well solution (1.9 M ammonium sulfite and 100 mM sodium acetate, pH 6.0). Crystals (~0.6 × 0.3 × 0.2 mm) were formed in 3–5 days in the

TABLE 1
Dissociation constants for wild type and Gly-to-Asp-substituted Gα subunit interactions with binding partners

K_D (μM)[a]	$G\alpha_{i1}$ wild type			$G\alpha_{i1}$ G202D		
	GDP	GTPγS	GDP · AlF_4^-	GDP	GTPγS	GDP · AlF_4^-
$G\beta_1\gamma_1$	1.75[b] (1.7–1.8)	38 (31–44)	NB[c]	1.9 (1.3–2.6)	2.8 (2.4–3.3)	2.1 (1.3–2.9)
PCP-2	0.84 (0.68–1.0)	NB	448 (130–760)	7.5 (3.7–11.3)	7.0 (4.6–9.3)	7.7 (4.7–10.8)
Ric-8A	0.39 (0.26–0.51)	356 (41–670)	107 (68–146)	4.1 (1.2–7.0)	5.5 (3.0–8.0)	3.6 (1.8–5.3)
RGS14 (RGS)	NB	310 (150–470)	0.08 (0.05–0.1)	NB	NB	NB
	$G\alpha_{t/i1}$ wild type			$G\alpha_{t/i1}$ G198D		
PDEγ (aa 63–87)	NB	ND[d]	5.21	NB	ND	NB

[a] Dissociation constants (K_D in micromolar) were determined using surface plasmon resonance spectroscopy (see representative SPR sensorgrams in Fig. 2). For experiments with $G\alpha_{i1}$, equilibrium resonance units of specific binding were graphed *versus* Gα concentration and fit to the equation $Y = (B_{max} \cdot X)/(K_D + X)$. Data are presented with 95% confidence intervals in parentheses. For $G\alpha_{t/i1}$/PDEγ experiments, affinity was calculated by kinetic analysis (S.E. in parentheses): $k_a = 1.6 \times 10^2$ (0.9) $M^{-1}\,s^{-1}$, $k_d = 8.33 \times 10^{-4}$ (0.1) s^{-1}.
[b] Note that the dissociation constant (K_D) established for the binding of His_6-$G\alpha_{i1}$ · GDP to immobilized $G\beta_1\gamma_1$ is higher than expected from comparable studies given our use of non-lipid-modified Gα and Gβγ subunits as well as a high concentration of free magnesium (Sarvazyan *et al.* 1998 JBC *273*:7934; Higashijima *et al.* 1987 JBC *262*:762).
[c] NB indicates no binding was observed.
[d] ND indicates that affinity was not determined.

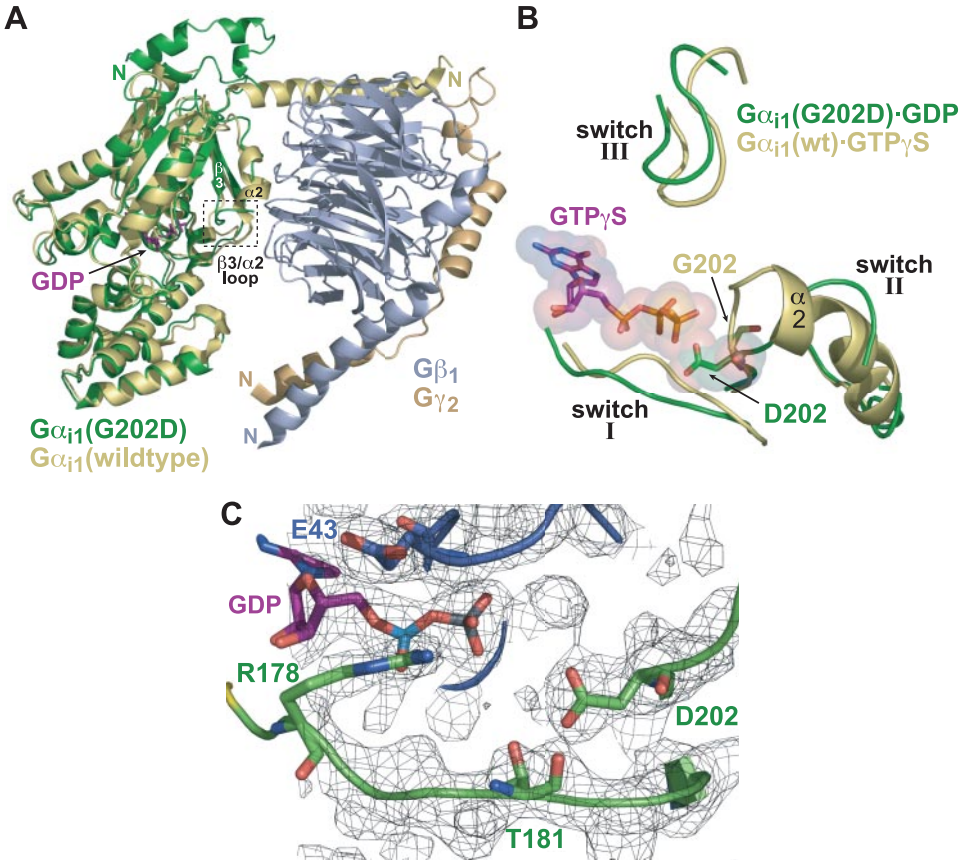

FIGURE 3. **Structural features of GDP-bound $G\alpha_{i1}$(G202D) compared with GDP-bound and GTPγS-bound wild type $G\alpha_{i1}$.** *A*, superposition of GDP-bound $G\alpha_{i1}$(G202D) (*green*) with wild type $G\alpha_{i1}$·GDP/$G\beta_1\gamma_2$ heterotrimer ($G\alpha_{i1}$ (*yellow*), $G\beta_1$ (*gray*), $G\gamma_2$ (*wheat*); Protein Data Bank code 1GP2). Aside from the N-terminal helix, $G\alpha_{i1}$(G202D) is largely unaltered compared with wild type. However, the β3/α2 loop containing the G202D mutation is displaced from the nucleotide-binding pocket relative to wild type, Gβγ-bound $G\alpha_{i1}$. The partially ordered switch II region that proceeds from the β3/α2 loop does not assume the helical nature typical of Gβγ-bound and activated conformations of Gα. *B*, superposition of $G\alpha_{i1}$(G202D)·GDP (*green*) and $G\alpha_{i1}$·GTPγS (*yellow*; Protein Data Bank code 1AS0). Switch I and III regions are in a similar orientation; however, the orientations of switch II differ dramatically, most notably in the N-terminal portion (*i.e.* the β3/α2 loop). In wild type Gα, binding of GTPγS induces a rigid helical conformation in switch II (α2) that results in its movement toward the nucleotide-binding pocket. However, in the G202D mutant, switch II is deflected away from the nucleotide. Importantly, the Asp^{202} side chain demonstrates a significant steric and electrostatic clash with the γ-phosphate of the modeled GTPγS molecule. *C*, depiction of the GDP-binding pocket illustrating the orientation of the Asp^{202} side chain relative to GDP. Notably the acidic side chain of Asp^{202} is oriented directly toward the β-phosphate of GDP. Residues of switch I critical for GTP hydrolysis (Arg^{178} and Thr^{181}) are shown along with Glu^{43} in the phosphate-binding loop region. The confidence of the structural model is highlighted by a $2F_o - F_c$ simulated annealing omit electron density map contoured at 1.0σ (*gray mesh*).

space group I4 ($a = b = 127.87$ Å, $c = 68.35$ Å, $\alpha = \beta = \gamma = 90$ °), with 1 molecule in the asymmetric unit. For data collection at 100 K, crystals were transferred to a solution containing well solution supplemented with 20% (w/v) glycerol for 90 s followed by immersion in liquid nitrogen. A native data set was collected on a single crystal using an R-Axis IV++ detector with Rigaku (The Woodlands, TX) rotating anode generator and osmic confocal "blue" optics at the University of North Carolina, Chapel Hill, x-ray facility. Diffraction data were scaled and indexed using HKL2000 (30). The structure of $G\alpha_{i1}$·GDP (Protein Data Bank code 1AS3), excluding residues 177–184 and 195–220, GDP, waters, and other heterogeneous molecules, was used as a molecular replacement model for $G\alpha_{i1}$(G202D) using Phaser in CCP4 (31). Model building was achieved using the programs O and Coot (32, 33). Model refinement was conducted using real space refinement protocols in Coot as well as a combination of rigid body, simulated annealing, energy minimization, and *b*-factor protocols in CNS (34). All structural images were made with PyMol (DeLano Scientific, San Carlos, CA).

Fluorescence Spectroscopy—Intrinsic tryptophan fluorescence was measured using an LS55 spectrometer (PerkinElmer Life Sciences). Excitation and emission wavelengths were 292 and 342 nm respectively, with slit widths of 2.5

nm. Fluorescence was measured in temperature-controlled cuvettes containing 1 ml of 10 mM Tris/HCl, pH 8.0, 1 mM EDTA, 5 mM $MgCl_2$, 150 mM NaCl. Controls were performed to account for any nonspecific effects of GTPγS addition on fluorescence.

Microscopy and Spindle Severing—Preparation of embryos, time-lapse differential interference contrast microscopy, and spindle severing were performed as described (10, 35, 36). Experiments were conducted using a homemade device that consists of a thermostat and a cooling/heating element coupled to a fan blowing air at the appropriate temperature onto the objective and the microscope stage. The temperature of the embryo during the experiment was monitored using a thermometer inserted in the agarose pad. Measurements of peak velocities of spindle poles following spindle severing were performed essentially as described (36).

RESULTS AND DISCUSSION

G202D Mutation Gives Temperature-dependent Lability to the Activated Gα State—We purified wild type and G202D $G\alpha_{i1}$ to homogeneity as assessed by SDS-PAGE (data not shown). $G\alpha_{i1}$(G202D)·GDP migrated in size exclusion chromatography as a monomer and had a circular dichroism spectrum consistent with properly folded Gα (data not shown) (37). We first tested the ability of purified $G\alpha_{i1}$ to bind nucleotide at 30 °C to approximate conditions found *in vivo* at the restrictive temperature. Wild type $G\alpha_{i1}$ bound GTPγS in a saturable manner with an association rate comparable with published values (38) (Fig. 1*A*). By contrast, $G\alpha_{i1}$(G202D) rapidly bound GTPγS but in a biphasic manner, peaking at 30 min then rapidly decaying over time. We also examined GTPγS binding at the permissive temperature (Fig. 1*B*). GTPγS binding by $G\alpha_{i1}$(G202D) at 15 °C was rapid, monophasic, and stable for up to 15 h. These data suggest that $G\alpha_{i1}$(G202D), and by extrapolation GPA-16(it143), undergoes nucleotide state-dependent inactivation at 30 °C but not 15 °C. The rate of GTPγS binding by $G\alpha_{i1}$(G202D) at 15 °C was over an order of magnitude faster than the wild type protein (Fig. 1*B*), suggesting that the G202D mutation also enhances spontaneous GDP release.

High spontaneous GDP release engendered by the G202D mutation may contribute to Gα inactivation at the restrictive temperature by promoting the GTP-bound form of the protein. Alternatively, it is well described that nucleotide-free Gα subunits are inherently unstable (20, 39, 40); thus, increased residence of Gα(G202D) in the nucleotide-free state could also contribute to inactivation. This is suggested to be the mechanism of temperature sensitivity of the human $G\alpha_s$(A366S) mutant, which bears an Ala-to-Ser point mutation in the GDP-binding pocket that increases spontaneous GDP release causing constitutive activity (40, 41). Uniquely, this mutation is permissive at the temperature of the human testis (32–33 °C) causing testotoxicosis because of the overproduction of testosterone. In other tissues, the protein is nonfunctional at 37 °C causing pseudohypoparathyroidism, typical of $G\alpha_s$ reduction of function (42).

Thermal melting of the $G\alpha_i$ family proteins under examination in this study gave a single cooperative transition from predominantly α-helical structure to random coil, as measured by circular dichroism. Normally, activated Gα is significantly more thermostable than inactive Gα; wild type $G\alpha_{i1}$·GDP had a melting temperature of 50 °C, whereas wild type $G\alpha_{i1}$·GTPγS had a melting temperature of 77 °C (Fig. 1*C*) consistent with structural data that the three switch regions of GDP-bound Gα are conformationally flexible, and GTPγS binding induces a distinct, stable switch region conformation (43). In contrast to wild type, GTPγS binding to $G\alpha_{i1}$(G202D) did not induce a thermostable protein-nucleotide complex; both GDP- and GTPγS-bound $G\alpha_{i1}$(G202D) had melting temperatures of 50 °C (Fig. 1*D*). These data suggest a mechanism for the temperature-sensitive loss-of-function in GPA-16(it143); at the permissive temperature, GPA-16(it143) is relatively stable in both the GDP- and GTP-bound forms, whereas at the restrictive temperature GPA-16(it143) is unstable in the GTP-bound state, becoming rapidly inactivated. Compatible with this view, the phenotype of *gpa-16*(*it143*) embryos at 25 °C is indistinguishable from that of embryos depleted of *gpa-16* by RNAi (9, 10).

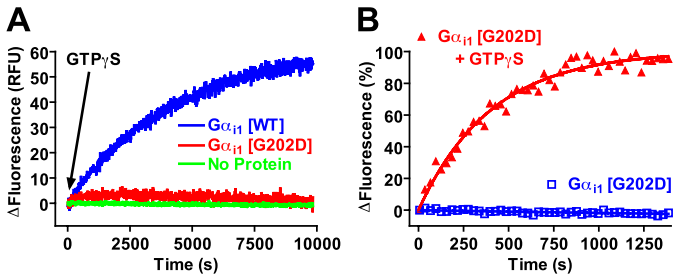

FIGURE 4. **The G202D mutation compromises proper switch II rearrangement upon GTPγS binding.** *A*, time course of $G\alpha_{i1}$ intrinsic tryptophan fluorescence enhancement by GTPγS. The intrinsic fluorescence of buffer (*No Protein*), 100 nM wild type (*WT*) $G\alpha_{i1}$, or 100 nM $G\alpha_{i1}$ (*G202D*) was measured at 30 °C. 100 μM GTPγS was added at 0 s as indicated by the *arrow*. *RFU* = relative fluorescence units. Data were fit to a single exponential association function to determine the activation rate constant (95% confidence intervals in parentheses): WT 0.0139 (0.0137–0.0142) min^{-1}. *B*, time course of $G\alpha_{i1}$(G202D) intrinsic tryptophan fluorescence enhancement by GTPγS. The intrinsic fluorescence of 100 nM $G\alpha_{i1}$(G202D) was measured at 30 °C. 100 μM GTPγS was added at 0 s, as denoted. Data were normalized to percentage change in fluorescence. Data were fit to a single exponential association curve (95% confidence interval in parentheses): G202D+GTPγS 0.149 (0.13–0.16) min^{-1}. Data from intrinsic tryptophan fluorescence experiments (as illustrated in *A* and *B*; $n = 3$ independent experiments) were also analyzed to determine mean percent fluorescence enhancement over GDP-bound basal state (with mean ± S.E. in parentheses as follows: wild type $G\alpha_{i1}$, 57% (±4%); $G\alpha_{i1}$(G202D), 4% (±1%).

G202D Mutation Perturbs Nucleotide-dependent Interactions with Gα Regulators—Gα switch regions are involved in mediating interactions with various Gα regulators that are important in ACD (7, 11, 43–48). We examined the ability of $G\alpha_{i1}$(G202D) to interact with cognate regulatory proteins, performing these experiments at 15 °C to ensure that stable $G\alpha_{i1}$(G202D) was operative in all cases. As assessed by surface plasmon resonance (SPR), wild type GDP-bound $G\alpha_{i1}$ exhibited robust interaction with immobilized, biotinylated $G\beta_1\gamma_1$ (Fig. 2*A*; Table 1), whereas GTPγS- and AlF_4^--bound wild type $G\alpha_{i1}$ had negligible binding, consistent with the known nucleotide state-selective association of Gα with Gβγ (49). In contrast, $G\alpha_{i1}$(G202D) exhibited strong interactions with $G\beta_1\gamma_1$ irrespective of nucleotide state (Fig. 2*B*; Table 1). These results suggest that the G202D mutation impairs the Gα switch region(s) from adopting the activated conformation in response to the ligands GTPγS and GDP·AlF_4^-.

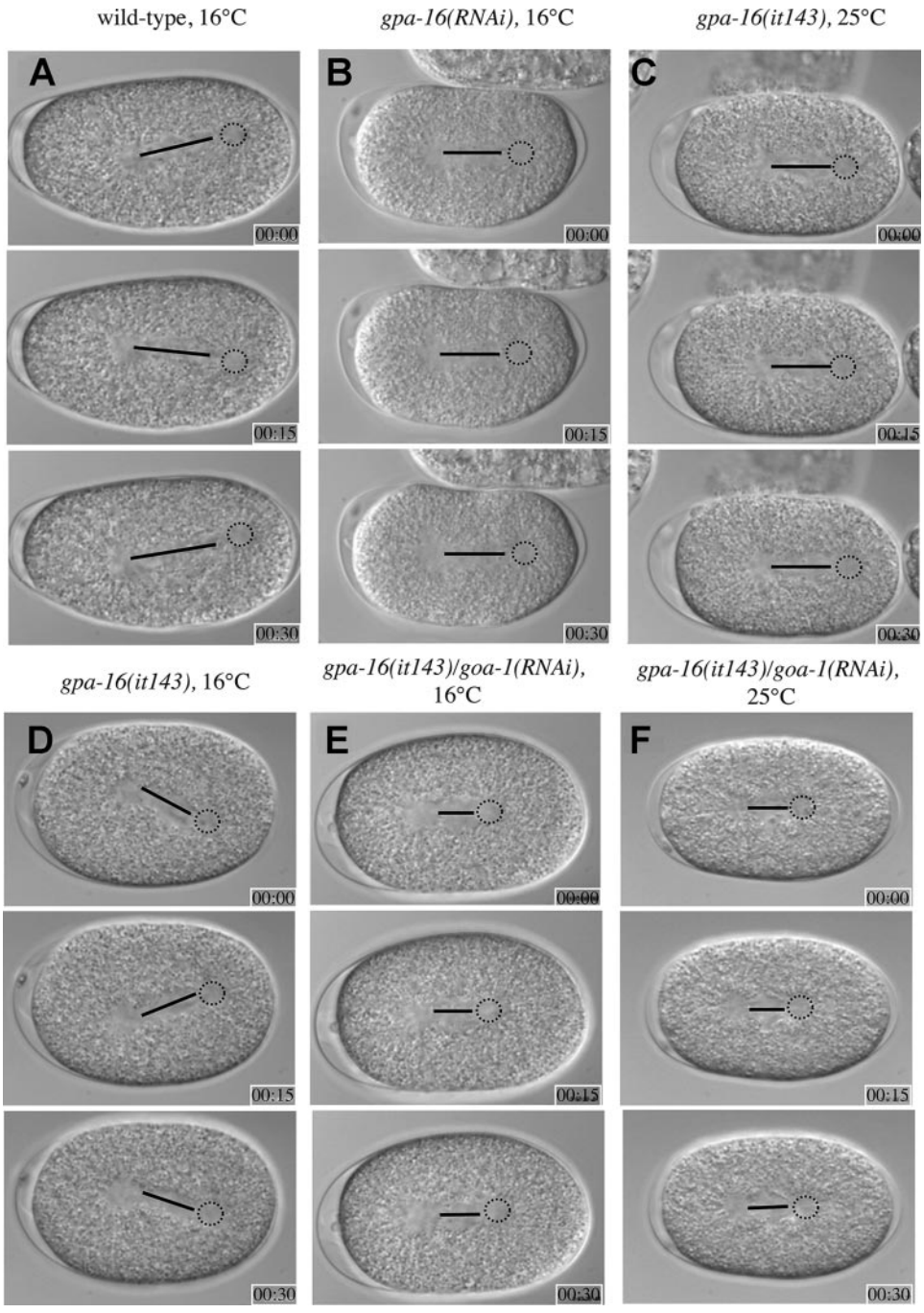

FIGURE 5. **Spindle oscillations occur normally in *gpa-16*(*it143*) but not *gpa-16*(*it143*)/*goa-1*(*RNAi*) embryos at 16 °C.** Images from time-lapse differential interference contrast microscopy of wild type (16 °C) (*A*), *gpa-16*(*RNAi*) (16 °C) (*B*), *gpa-16*(*it143*) (25 °C) (*C*), *gpa-16*(*it143*) (16 °C) (*D*), *gpa-16*(*it143*)/*goa-1*(*RNAi*) (16 °C) (*E*), and *gpa-16*(*it143*)/*goa-1*(*RNAi*) (25 °C) (*F*) embryos during anaphase (see corresponding supplemental movies 1–6). *Black lines* depict the distance between the two centrosomes of the spindles, and the *dashed circles* indicate the position of the posterior spindle pole. Elapsed time is indicated in minutes and seconds; embryos are about 50 μm long, and anterior is to the left, posterior to the right. Note that spindle oscillations occur in both wild type and *gpa-16*(*it143*) embryos at 16 °C, but not in embryos of the other genotypes (*B, C, E,* and *F*).

Wild type $G\alpha_{i1}$ also exhibited GDP-specific binding to the GoLoco motif protein PCP-2 and the guanine nucleotide exchange factor Ric-8A (Fig. 2, *C* and *E*; Table 1), consistent with previous studies (9, 17, 20). In contrast, $G\alpha_{i1}$(G202D) interacted in a nucleotide-independent manner with PCP-2 and Ric-8A (Fig. 2, *D* and *F*), and with markedly reduced affinities *versus* wild type $G\alpha_{i1}$·GDP (K_D for PCP-2 of 7–8 μM *versus* 800 nM, K_D for Ric-8A of 4–5 μM *versus* 400 nM; Table 1). We and others have previously shown RGS14 and $G\alpha_i$ subunits to be involved in mammalian spindle formation and orientation (reviewed in Refs. 1, 5). Whereas wild type $G\alpha_{i1}$ exhibited a high affinity, AlF_4^--dependent interaction with the RGS14 RGS domain (Fig. 2*G*) as shown previously (22), no binding was observed between any form of $G\alpha_{i1}$(G202D) and RGS14 (Fig. 2*H*). As RGS domains and $G\alpha$ effectors bind distinct (44), but at times overlapping (50), regions of switch II, we examined if the G202D mutation also altered effector binding in the context of a chimeric transducin/$G\alpha_{i1}$ protein ($G\alpha_{t/i1}$) (18) known to exhibit activation-dependent binding to a fragment of the γ subunit of cGMP PDEγ (23). Wild type $G\alpha_{t/i1}$ bound, in an activation-dependent manner, to immobilized PDEγ peptide as expected (Fig. 2*I*; Table 1); however, no binding was seen between ground state (nor activated) $G\alpha_{t/i1}$(G198D) and PDEγ (Fig. 2*J*; Table 1), suggesting that the Gly-to-Asp substitution abrogated the effector binding properties of $G\alpha_{t/i1}$.

GPA-16(it143) Interacts with GPR-1/-2 and RIC-8 in a Nucleotide-independent Manner—The binding studies detailed above establish that the G202D mutation within switch II renders $G\alpha$ unable to interact properly *in vitro* with many $G\alpha$ regulators, including those that bind activated states (*i.e.* RGS domains, effectors). We confirmed that GPA-16(it143) exhibits this lack of proper nucleotide state-selective interactions by co-immunoprecipitation using *C. elegans* embryo extracts. Using this approach, we previously showed that wild type GPA-16 interacts robustly with the GoLoco motif proteins GPR-1/-2 in the presence of GDP but much less so in the presence of GTPγS, whereas wild type GPA-16 interacts with RIC-8 equally well in the presence of either nucleotide (9). Here we used embryonic extracts from worms grown at 16 °C and conducted co-immunoprecipitation at 16 °C to investigate the behavior of native complexes at the permissive temperature. The interaction between GPA-16(it143) and GPR-1/-2 was decreased compared with wild

type GPA-16, whereas that between GPA-16(it143) and RIC-8 was not diminished (Fig. 1*E*). The interaction between GPA-16(it143) and GPR-1/-2 occurred equally well in the presence of GDP or GTPγS, in contrast to wild type GPA-16 (Fig. 1*E*). This finding is compatible with the *in vitro* results of Table 1 and supports the view that GPA-16(it143)·GDP and GPA-16(it143)·GTP can both associate with GPR-1/-2 at the permissive temperature *in vivo*. Overall, these findings suggest that the G202D substitution renders Gα proteins unable to interact properly *in vivo* with their regulatory proteins.

Structural Changes Caused by the G202D Mutation—We determined the crystal structure of $G\alpha_{i1}$(G202D)·GDP to 2.2 Å (Fig. 3; supplemental Table 1). The overall structure of $G\alpha_{i1}$(G202D) is largely unaltered from wild type $G\alpha_{i1}$ (51) with an overall root mean square deviation of 0.38 Å (Fig. 3*A*). Surprisingly, switch I and III of GDP-bound $G\alpha_{i1}$(G202D) adopt conformations similar to those of *activated* conformations of Gα (Fig. 3*B*). Arg^{178} and Thr^{181}, important residues to GTP hydrolysis found in switch I (51), do not undergo significant alterations in side-chain conformation compared with activated Gα structures, despite a slight alteration in the switch I backbone conformation (Fig. 3*B* and data not shown). The conformation of switch II is unique and likely a direct result of the G202D mutation. Although residues Lys^{208}–Trp^{211} of switch II are disordered, the β3/α2 loop (within which the G202D mutation resides) folds back toward the α2/α3 cleft and away from the nucleotide pocket (Fig. 3*A*). This altered conformation may underlie enhanced spontaneous GDP release seen with the G202D mutant (Fig. 1*B*), as the β3/α2 loop is thought to be an occlusive barrier to the release of GDP (2). Additionally, the orientation of the Asp^{202} side chain toward GDP (Fig. 3*C*) may introduce an electrostatic repulsion causing enhanced GDP release. Although the Asp^{202} side chain orients directly at the GDP β-phosphate, the distance separating its electronegative carboxylate from the β-phosphate (~5 Å) is great enough to prevent an outright electrostatic or steric clash. However, GTP binding would present significant electrostatic and steric clashes with the Asp^{202} side chain (Fig. 3*B*). Such a clash may lead to protein instability, an effect likely exacerbated at elevated temperatures.

We also measured Gα conformational change upon activation by GTPγS. Gα subunits contain a tryptophan in switch II (Trp^{211} in $G\alpha_{i1}$ and GPA-16) that shifts from being solvent-exposed when GDP is bound to a hydrophobic pocket when GTPγS is bound (reviewed in Ref. 52). Wild type $G\alpha_{i1}$ gave a substantial increase in Trp fluorescence upon exposure to GTPγS (Fig. 4*A*); in contrast, $G\alpha_{i1}$(G202D) gave a minimal increase in fluorescence upon incubation with GTPγS (Fig. 4*A*). This weak fluorescence enhancement was reproducible and specific (Fig. 4*B*), albeit severely diminished in magnitude (4% increase over GDP-bound basal fluorescence *versus* 57% increase of wild type).

Taken together, these findings indicate that $G\alpha_{i1}$(G202D) alters the conformation of switch II in response to GTPγS binding, most likely by preventing complete rotation and translation toward the GTP-binding pocket (53, 54). Combined with the observation that switch I and III conformations in $G\alpha_{i1}$(G202D)·GDP are similar to activated $G\alpha_{i1}$, the G202D-induced changes in switch II conformation help resolve not only the reduced affinity of $G\alpha_{i1}$(G202D) seen for certain binding partners (*e.g.* PCP-2, Ric-8A, and RGS14; Table 1) but also the loss of nucleotide selectivity for such interactions (Fig. 2).

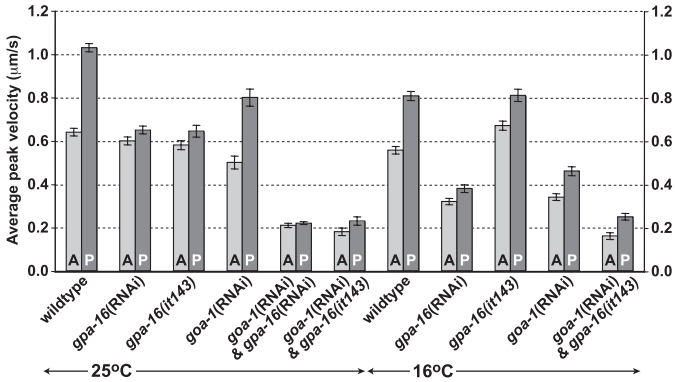

FIGURE 6. **Pulling forces on spindle poles at 16 °C are normal in *gpa-16(it143)* but not *gpa-16(it143)/goa-1*(RNAi) embryos.** Average peak velocities of the anterior (*A*) and posterior (*P*) spindle poles (±S.E.) following spindle severing of *C. elegans* embryos of the indicated genotypes. Experiments were performed as indicated either at 16 °C (this study) or at 25 °C (as previously described in Refs. 7, 9, 10 or in this study for *gpa-16*(*it143*)*/goa-1*(RNAi) embryos). For values and statistical tests, see supplemental Table 2.

Normal Pulling Forces Seen at the Permissive Temperature in gpa-16(it143) Embryos Are GOA-1-dependent—We also evaluated the consequences of the G202D mutation on GPA-16 function *in vivo* by analyzing pulling forces on astral microtubules in *gpa-16*(*it143*) embryos at 16 °C. In wild type embryos, the posterior aster undergoes characteristic oscillations transverse to the longitudinal axis, reflecting the extent of pulling forces acting on the spindle poles (Fig. 5*A* and supplemental movie 1) (7). Although oscillations are largely abolished in *gpa-16*(*it143*) embryos at 25 °C (Fig. 5*C* and supplemental movie 3) (9), they are indistinguishable from wild type oscillations in *gpa-16*(*it143*) embryos at 16 °C (Fig. 5*D* and supplemental movie 4), suggesting that pulling forces are intact at the permissive temperature. We conducted *in vivo* laser microbeam-mediated spindle severing to reveal the extent of net pulling forces acting on each spindle pole (36). Pulling forces in wild type embryos were reduced at 16 °C compared with 25 °C (Fig. 6 and supplemental Table 2), presumably a reflection of a global slowing at the lower temperature of biochemical reactions, such as microtubule dynamics known to be important for pulling force generation (14). However, net pulling forces were not decreased in *gpa-16*(*it143*) embryos at 16 °C compared with 25 °C and, more surprisingly, were even slightly increased on the anterior spindle pole in comparison with wild type at 16 °C (Fig. 6). Intact pulling forces in *gpa-16*(*it143*) embryos at 16 °C cannot be ascribed to GPA-16 being dispensable for pulling forces at this temperature, because *gpa-16*(*RNAi*) embryos at 16 °C did not exhibit oscillations (supplemental Movie 2, Fig. 5*B*, and supplemental movie 2) and had decreased pulling forces (Fig. 6).

To test whether normal pulling forces at 16 °C in *gpa-16*(*it143*) embryos may be sustained by GOA-1 function, given that GPA-16 and GOA-1 are partially redundant for force generation (8), we inactivated *goa-1* using RNAi in *gpa-16*(*it143*) embryos. Oscillations were absent and pulling forces substan-

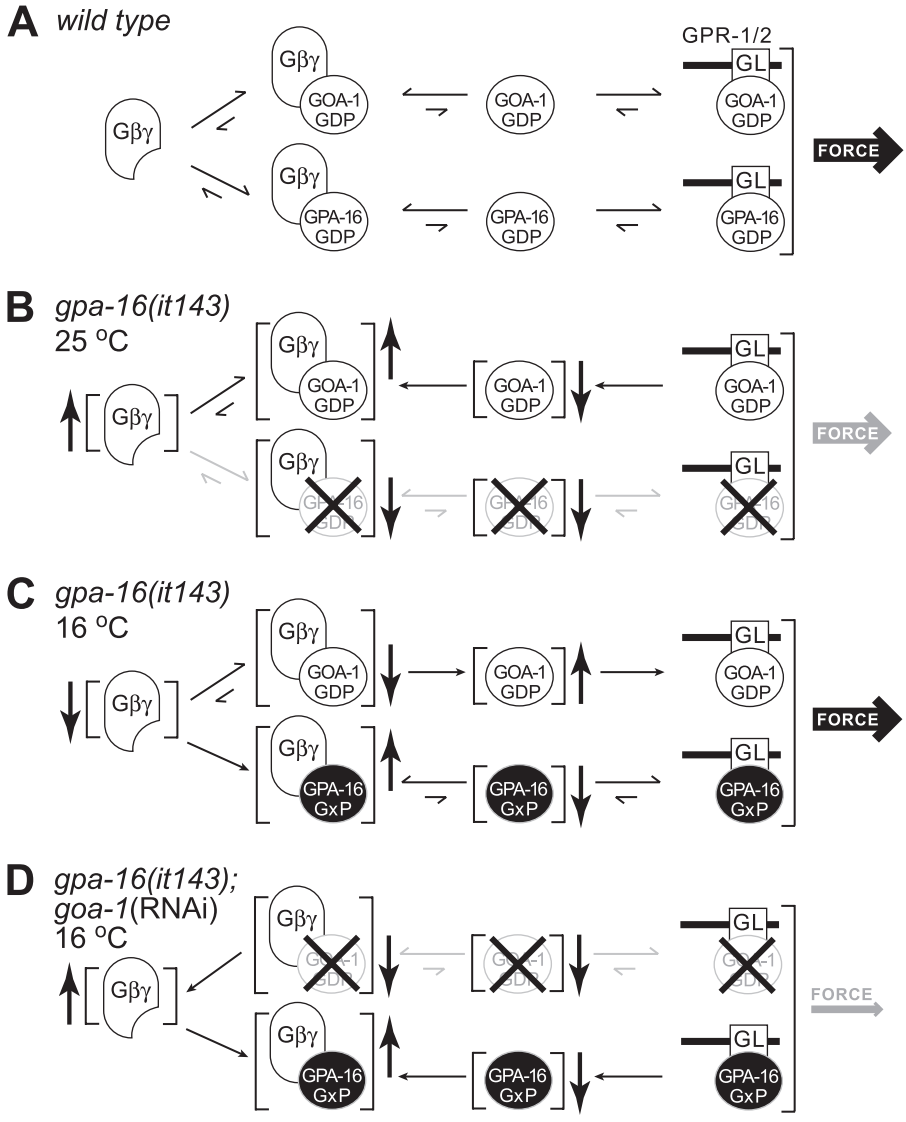

FIGURE 7. **A model for heterotrimeric G-protein function during *C. elegans* asymmetric cell division and functions of the GPA-16(it143) temperature-sensitive mutant at both the restrictive and permissive temperatures.** *A,* this model, based on published data (7, 9, 10), assumes that Gα·GDP bound to GPR-1/2 is crucial for pulling force generation. In the wild type embryo, GOA-1·GDP and GPA-16·GDP interact with the GoLoco motif ("*GL*") proteins GPR-1/2 at the cell cortex to mediate pulling forces. Gα·GDP/GPR-1/2 concentration is determined by an equilibrium between the levels of free Gα·GDP, the amount of free Gβγ, and the amount of Gα·GDP/Gβγ. For simplicity, we have omitted from this model other regulatory components that likely participate such as RIC-8 (10), RGS-7 (11), and LIN-5 (55). *B,* GPA-16(it143) is unstable at 25 °C and likely misfolds or has defects in tertiary structure. Loss of functional GPA-16(it143) prevents the formation of GPA-16·GDP/GPR-1/2, thereby decreasing pulling forces. Although not formally tested, it is possible that the loss of functional GPA-16(it143) protein may also lead to an increase in free Gβγ subunits, as illustrated here. This would increase the amount of GOA-1·GDP/Gβγ and consequently reduce the amount of GOA-1·GDP/GPR-1/2, thus decreasing pulling forces. *C,* GPA-16(it143) is stable at 16 °C and has lost the normal nucleotide-state dependence in its Gβγ and GoLoco motif interactions (denoted "*GxP*"; see Figs. 1*E* and 2 and Table 1). This leads to an increased amount of GPA-16/Gβγ, thereby reducing the amount of free Gβγ available for formation of GOA-1·GDP/Gβγ. The consequence of this is an increase in free GOA-1·GDP, a resultant increase in the amount of GOA-1·GDP/GPR-1/2, and thus increased pulling forces. (Although a strong nucleotide-independent interaction of GPA-16(it143) with Gβγ likely explains the observed phenotype at the permissive temperature, we cannot formally rule out that GPA-16(it143) alone (freed of Gβγ sequestration) may be competent for generating pulling forces. This notion is particularly interesting as GPA-16(it143) has appreciable, although nucleotide-state independent, binding to regulatory proteins such as RIC-8 and GPR-1/2. Thus, it is also possible that increased levels of GPA-16/GPR-1/2 at the permissive temperature may cause increased pulling forces.) *D,* loss of all GOA-1 protein by RNA interference prevents accumulation of GOA-1·GDP/GPR-1/2, thus decreasing pulling forces. Furthermore, increased amounts of free Gβγ sequesters the stable GPA-16(it143) mutant and prevents formation of GPA-16/GPR-1/2 complexes. Thus pulling forces are potentially reduced by two mechanisms.

tially diminished in such embryos at 16 °C (Fig. 5, *E* and *F*, and Fig. 6; supplemental Table 2). Thus, the pulling forces observed in *gpa-16*(*it143*) embryos at the permissive temperature are entirely GOA-1-dependent. One likely possibility is that GPA-16(it143) at 16 °C has a dominant interfering function, trapping a negative regulator of force generation and thus allowing GOA-1 to generate more extensive pulling forces than normally found in the wild type embryo. As suggested by our biochemical and structural analyses, GPA-16(it143) may be permanently bound to Gβγ because of its inability to change switch II conformation upon GTP binding. Thus, at 16 °C, GPA-16(it143) could act to sequester Gβγ (Fig. 7). Compatible with this view, pulling forces on the anterior spindle pole in *gpa-16*(*it143*) embryos at 16 °C are even slightly higher than in wild type embryos, a phenotype reminiscent of depletion of the Gβ subunit GPB-1 (9, 10). The relationship between total levels of Gα and Gβγ is crucial for pulling forces, as depletion of GPB-1 alone or in combination with either GOA-1 or GPA-16 results in exaggerated pulling forces (9). Thus, at the permissive temperature, *gpa-16*(*it143*) may be thought of as a gain-of-function allele that increases the amount of GOA-1 freed from Gβγ, thus leading to higher pulling forces.

Conclusions—Our structural, biochemical, and cell biological findings collectively suggest that, at the permissive temperature, GPA-16(it143) is stable but unable to interact properly with crucial regulators, leading to a dominant effect on the Gα-dependent force-generating pathway (Fig. 7). In contrast, at the restrictive temperature, our biochemical and functional analyses suggest that GTP binding destabilizes the protein, leading to a loss of activity. Moreover, enhanced spontaneous GDP release by the G202D mutation may contribute to inactivation at the restrictive temperature by promoting either the nucleotide-free form known to be highly unstable (39, 40) or the GTP-bound form, which we show here is also unstable at high temperature. Overall, at the restrictive temperature, *gpa-16*(*it143*) likely behaves as a null allele (Fig. 7*B*). Accordingly, *gpa-16*(*it143*) embryos at the restrictive temperature

exhibit a clear reduction in pulling forces much like *gpa-16*(*RNAi*) embryos (9, 10). Future studies will help to further clarify the differential biochemistry and spatiotemporal dynamics of GPA-16 and GOA-1 in *C. elegans* embryos and thus better illuminate the conserved actions of Gα subunits in governing ACD across metazoan evolution.

Acknowledgments—We thank Ashutosh Tripathy for assistance with CD, Alex Singer and John Sondek for helpful discussions, and Keith Jones for a reprint.

REFERENCES

1. Siderovski, D. P., and Willard, F. S. (2005) *Int. J. Biol. Sci.* **1,** 51–66
2. Johnston, C. A., and Siderovski, D. P. (2007) *Mol. Pharmacol.* **72,** 219–230
3. Betschinger, J., and Knoblich, J. A. (2004) *Curr. Biol.* **14,** R674–R685
4. Hampoelz, B., and Knoblich, J. A. (2004) *Cell* **119,** 453–456
5. Willard, F. S., Kimple, R. J., and Siderovski, D. P. (2004) *Annu. Rev. Biochem.* **73,** 925–951
6. Bellaiche, Y., and Gotta, M. (2005) *Curr. Opin. Cell Biol.* **17,** 658–663
7. Colombo, K., Grill, S. W., Kimple, R. J., Willard, F. S., Siderovski, D. P., and Gönczy, P. (2003) *Science* **300,** 1957–1961
8. Gotta, M., and Ahringer, J. (2001) *Nat. Cell Biol.* **3,** 297–300
9. Afshar, K., Willard, F. S., Colombo, K., Siderovski, D. P., and Gönczy, P. (2005) *Development* (*Camb.*) **132,** 4449–4459
10. Afshar, K., Willard, F. S., Colombo, K., Johnston, C. A., McCudden, C. R., Siderovski, D. P., and Gönczy, P. (2004) *Cell* **119,** 219–230
11. Hess, H. A., Roper, J. C., Grill, S. W., and Koelle, M. R. (2004) *Cell* **119,** 209–218
12. Tall, G. G., and Gilman, A. G. (2005) *Proc. Natl. Acad. Sci. U. S. A.* **102,** 16584–16589
13. Du, Q., and Macara, I. G. (2004) *Cell* **119,** 503–516
14. Nguyen-Ngoc, T., Afshar, K., and Gonczy, P. (2007) *Nat. Cell Biol.* **9,** 1294–1302
15. Bergmann, D. C., Lee, M., Robertson, B., Tsou, M. F., Rose, L. S., and Wood, W. B. (2003) *Development* (*Camb.*) **130,** 5731–5740
16. Willard, F. S., Kimple, A. J., Johnston, C. A., and Siderovski, D. P. (2005) *Anal. Biochem.* **340,** 341–351
17. Willard, F. S., McCudden, C. R., and Siderovski, D. P. (2006) *Cell. Signal.* **18,** 1226–1234
18. Pereira, R., and Cerione, R. A. (2005) *J. Biol. Chem.* **280,** 35696–35703
19. Willard, F. S., and Siderovski, D. P. (2004) *Methods Enzymol.* **389,** 320–338
20. Tall, G. G., Krumins, A. M., and Gilman, A. G. (2003) *J. Biol. Chem.* **278,** 8356–8362
21. Snyder, J. T., Singer, A. U., Wing, M. R., Harden, T. K., and Sondek, J. (2003) *J. Biol. Chem.* **278,** 21099–21104
22. Kimple, R. J., De Vries, L., Tronchere, H., Behe, C. I., Morris, R. A., Gist Farquhar, M., and Siderovski, D. P. (2001) *J. Biol. Chem.* **276,** 29275–29281
23. Johnston, C. A., Lobanova, E. S., Shavkunov, A. S., Low, J., Ramer, J. K., Blaesius, R., Fredericks, Z., Willard, F. S., Kuhlman, B., Arshavsky, V. Y., and Siderovski, D. P. (2006) *Biochemistry* **45,** 11390–11400
24. Brenner, S. (1974) *Genetics* **77,** 71–94
25. Mergny, J. L., and Lacroix, L. (2003) *Oligonucleotides* **13,** 515–537
26. Akima, H. (1970) *J. Assoc. Comp. Mach.* **17,** 589–602
27. Snow, B. E., Brothers, G. M., and Siderovski, D. P. (2002) *Methods Enzymol.* **344,** 740–761
28. McCudden, C. R., Willard, F. S., Kimple, R. J., Johnston, C. A., Hains, M. D., Jones, M. B., and Siderovski, D. P. (2005) *Biochim. Biophys. Acta* **1745,** 254–264
29. Willard, F. S., Low, A. B., McCudden, C. R., and Siderovski, D. P. (2007) *Cell. Signal.* **19,** 428–438
30. Otwinowski, Z., and Minor, W. (1997) *Methods Enzymol.* **276,** 307–326
31. Storoni, L. C., McCoy, A. J., and Read, R. J. (2004) *Acta Crystallogr. Sect. D Biol. Crystallogr.* **60,** 432–438
32. Emsley, P., and Cowtan, K. (2004) *Acta Crystallogr. Sect. D Biol. Crystallogr.* **60,** 2126–2132
33. Jones, T. A., Zou, J. Y., Cowan, S. W., and Kjeldgaard, M. (1991) *Acta Crystallogr. Sect. A* **47,** 110–119
34. Brunger, A. T., Adams, P. D., Clore, G. M., DeLano, W. L., Gros, P., Grosse-Kunstleve, R. W., Jiang, J. S., Kuszewski, J., Nilges, M., Pannu, N. S., Read, R. J., Rice, L. M., Simonson, T., and Warren, G. L. (1998) *Acta Crystallogr. Sect. D Biol. Crystallogr.* **54,** 905–921
35. Gönczy, P., Schnabel, H., Kaletta, T., Amores, A. D., Hyman, T., and Schnabel, R. (1999) *J. Cell Biol.* **144,** 927–946
36. Grill, S. W., Gönczy, P., Stelzer, E. H., and Hyman, A. A. (2001) *Nature* **409,** 630–633
37. Streiff, J., Warner, D. O., Klimtchuk, E., Perkins, W. J., Jones, K., and Jones, K. A. (2004) *Anesth. Analg.* **98,** 660–667
38. Linder, M. E., Ewald, D. A., Miller, R. J., and Gilman, A. G. (1990) *J. Biol. Chem.* **265,** 8243–8251
39. Chidiac, P., Markin, V. S., and Ross, E. M. (1999) *Biochem. Pharmacol.* **58,** 39–48
40. Posner, B. A., Mixon, M. B., Wall, M. A., Sprang, S. R., and Gilman, A. G. (1998) *J. Biol. Chem.* **273,** 21752–21758
41. Iiri, T., Herzmark, P., Nakamoto, J. M., van Dop, C., and Bourne, H. R. (1994) *Nature* **371,** 164–168
42. Spiegel, A. M., and Weinstein, L. S. (2004) *Annu. Rev. Med.* **55,** 27–39
43. Wall, M. A., Posner, B. A., and Sprang, S. R. (1998) *Structure* (*Lond.*) **6,** 1169–1183
44. Slep, K. C., Kercher, M. A., He, W., Cowan, C. W., Wensel, T. G., and Sigler, P. B. (2001) *Nature* **409,** 1071–1077
45. Kimple, R. J., Kimple, M. E., Betts, L., Sondek, J., and Siderovski, D. P. (2002) *Nature* **416,** 878–881
46. Tesmer, J. J., Sunahara, R. K., Gilman, A. G., and Sprang, S. R. (1997) *Science* **278,** 1907–1916
47. Tesmer, V. M., Kawano, T., Shankaranarayanan, A., Kozasa, T., and Tesmer, J. J. (2005) *Science* **310,** 1686–1690
48. Zwaal, R. R., Ahringer, J., van Luenen, H. G., Rushforth, A., Anderson, P., and Plasterk, R. H. (1996) *Cell* **86,** 619–629
49. Sarvazyan, N. A., Lim, W. K., and Neubig, R. R. (2002) *Biochemistry* **41,** 12858–12867
50. Hepler, J. R., Berman, D. M., Gilman, A. G., and Kozasa, T. (1997) *Proc. Natl. Acad. Sci. U. S. A.* **94,** 428–432
51. Coleman, D. E., Berghuis, A. M., Lee, E., Linder, M. E., Gilman, A. G., and Sprang, S. R. (1994) *Science* **265,** 1405–1412
52. Kimple, R. J., Jones, M. B., Shutes, A., Yerxa, B. R., Siderovski, D. P., and Willard, F. S. (2003) *Comb. Chem. High Throughput Screen* **6,** 399–407
53. Mixon, M. B., Lee, E., Coleman, D. E., Berghuis, A. M., Gilman, A. G., and Sprang, S. R. (1995) *Science* **270,** 954–960
54. Lambright, D. G., Sondek, J., Bohm, A., Skiba, N. P., Hamm, H. E., and Sigler, P. B. (1996) *Nature* **379,** 311–319
55. Srinivasan, D. G., Fisk, R. M., Xu, H., and van den Heuvel, S. (2003) *Genes Dev.* **17,** 1225–1239